BMC Cardiovascular Disorders

RESEARCH

Open Access

# A morphological indicator for aortic dissection: fitting circle of the thoracic aorta

Hongji Pu[1†], Tao Peng[2†], Zhijue Xu[1,3†], Qi Sun[4], Zixin Wang[2], Hui Ma[2], Shu Fang[2], Yang Yang[5], Jie Wu[6], Ruihua Wang[1], Peng Qiu[1*], Jinhua Zhou[2*] and Xinwu Lu[1*]

## Abstract

**Background** This study aims to identify a morphological indicator of aortic dissection (AD) based on the geometrical characteristics of the thoracic aorta.

**Methods** We evaluated computed tomographic angiograms of 63 samples with AD (22 with type A AD, 41 with type B AD) and 71 healthy samples. Via centerline extraction and spatial transformation, the spatial entanglement of the aorta was minimized, and the expanded 2D aortic morphology was obtained. The 2D morphology of the thoracic aorta was fit to a circle. The applicability of the fitting circle method for identifying aortic dissection was verified by multivariable logistic regression analysis.

**Results** Via the 3D coordinate transformation algorithm, the optimal aortic view was obtained. On this view, the geometrical characteristics of the thoracic aortas of the healthy controls were similar to a portion of a circle (sum of residuals: 3502.45 ± 2566.71, variance: 86.23 ± 56.60), while that of AD samples had poorer similarity to the circle (sum of residuals: 5404.78 ± 3891.69, variance: 129.90 ± 90.09). This difference was significant ($p < 0.001$). A logistic regression model showed that increased deformation of the thoracic aorta was a significant indicator of aortic dissection (odds ratio: 1.35, $p = 0.034$).

**Conclusions** The morphology of the healthy thoracic aorta could be fit to a circle, while that of the dissected aorta had poorer similarity to the circle. The statistics of the circle are an effective indicator of aortic deformation in AD.

**Trial registration** This study is registered in the Chinese Clinical Trial Registry (ChiCTR2000029219).

**Keywords** Aortic dissection, Computed tomographic angiography, Geometrical analysis, Diagnostic imaging, Algorithm

†Hongji Pu, Tao Peng and Zhijue Xu these authors contributed equally to this work.

*Correspondence:
Peng Qiu
hiiigh@163.com
Jinhua Zhou
zhoujinhua@ahmu.edu.cn
Xinwu Lu
luxinwu@shsmu.edu.cn
[1] Department of Vascular Surgery, Shanghai Ninth People's Hospital, Shanghai Jiao Tong University School of Medicine, Shanghai 200011, China
[2] School of Biomedical Engineering, Anhui Medical University, Meishan Road, Shushan District, Hefei 230032, China
[3] Key Laboratory of Systems Biomedicine (Ministry of Education), Shanghai Center for Systems Biomedicine, Shanghai Jiao Tong University, Shanghai 200240, China
[4] Department of Radiology, Shanghai Ninth People's Hospital, Shanghai Jiao Tong University School of Medicine, Shanghai 200011, China
[5] Department of Computer Science and Engineering, Shanghai Jiao Tong University, Shanghai 200240, China
[6] Department of Vascular Surgery, Affiliated Hospital of Guizhou Medicine University, Guizhou 550000, China

© The Author(s) 2024. **Open Access** This article is licensed under a Creative Commons Attribution-NonCommercial-NoDerivatives 4.0 International License, which permits any non-commercial use, sharing, distribution and reproduction in any medium or format, as long as you give appropriate credit to the original author(s) and the source, provide a link to the Creative Commons licence, and indicate if you modified the licensed material. You do not have permission under this licence to share adapted material derived from this article or parts of it. The images or other third party material in this article are included in the article's Creative Commons licence, unless indicated otherwise in a credit line to the material. If material is not included in the article's Creative Commons licence and your intended use is not permitted by statutory regulation or exceeds the permitted use, you will need to obtain permission directly from the copyright holder. To view a copy of this licence, visit http://creativecommons.org/licenses/by-nc-nd/4.0/.

## Background

Aortic dissection (AD) is one of the most common fatal aortic diseases, responsible for the deaths of approximately 30% of patients with type A AD and 10% of patients with type B AD before they can even arrive to the hospital [1, 2]. It is important to find a way to visually identify dissected aortas rapidly and quantifiably [3–5].

The pathological changes in AD can occur not only near the proximal tear but also throughout the entire aorta. The thoracic aorta is responsible for transporting blood and absorbing the ejection kinetic energy of the heart [6, 7]. The main reason for aortic dissection is an unbalanced transformation from the kinetic energy of blood flow to the elastic potential energy of the aortic wall. This imbalance leads to tear out of the aortic intima [8, 9]. According to previous studies, abnormal thoracic aorta shapes correlated with the abnormality of the aortic wall structure and hemodynamic stress [8–10]. Whether the biological cause of AD is an intima tear or media necrosis, macroscopic deformation of the aorta can be observed by imaging [11, 12].

In addition to the diameter of the aorta, other comprehensive imaging-based indexes are required to describe the risk of AD. Although aortic diameter greater than 5.5 cm is a recognized risk factor for AD [1], more than 60% of type A ADs and more than 80% of type B ADs occur in patients with normal-diameter aortas according to the IRAD global data [13, 14]. Recently, the length of the thoracic aorta was considered another morphological risk factor for thoracic AD [15, 16]. However, this indicator alone is also unable to describe the overall shape of the thoracic aorta [17]. According to previous studies, aortic tortuosity has been confirmed to be related to aortic dissection onset, which may be a manifestation of abnormal aortic histology. Additionally, it can induce abnormal hemodynamics and affect the aorta [18]. Sharper angulation and higher tortuosity of the aortic arch are considered geometric factors associated with aortic dissection [19, 20]. Our previous study confirmed that type B AD is related to the deformation of the arch and the proximal descending aorta. The deformation related to the dissection tends to be wider and inclined, and the dissected aorta appears slumped overall, and angulated and stiff locally [21]. Therefore, the tortuosity and slumpedness of the thoracic aorta may be indexes for AD, and it is desirable to find a method to quantify differences between dissected and healthy thoracic aortas.

To quantitatively describe the characteristics of the aorta, computed tomography angiography (CTA) images need to be transformed using methods including three-dimensional (3D) reconstruction and centerline extraction of the aorta. In our previous study, a 3D rotation projection modeling method was established to determine the optimal projection plane [3]. On this optimal projection plane, the morphological features of the thoracic aorta were extracted. This algorithm reduced the complexity of 3D morphological analysis and allowed the use of reproducible and quantificational parameters to describe the centerline extracted from CTA instead of subjective judgment.

Based on the previous works, an additional algorithm is needed to describe healthy and dissected aortas by quantitatively describing and identifying the characteristics of the aorta in AD. The morphology of the thoracic aorta was described by the difference between the aortic centerline and a fitted circle. The correlation between the fitted circle and AD was then verified using multivariable logistic regression analysis.

## Methods

Figure 1 demonstrates the principal steps of the procedure in the study. Three-dimensional reconstruction of the aorta was performed with CTA data. The lumen centerline of the reconstructed aorta and the corresponding coordinates were extracted. The optimal aortic view was obtained via the 3D coordinate transformation algorithm, and the two-dimensional (2D) morphology was subjected to circle fitting. The applicability of the fitting circle method for the identification of AD was verified by multivariable logistic regression analysis.

### Population

This study is a retrospective multicenter cross-sectional study. Imaging data were retrospectively retrieved from the medical records of patients with continuous Stanford type A or B aortic dissection who underwent chest CTA examination in the two centers from January 2017 to December 2018 and were included in the dissection group. The exclusion criteria for the dissection group were as follows: (1) connective tissue disease (Marfan's disease, Loeys–Dietz syndrome or Ehlers–Danlos syndrome, etc.); (2) iatrogenic dissection; (3) other aortic diseases, such as aneurysms; (4) previous aortic surgery; (5) a previous cardiothoracic disease or cardiothoracic surgery; (6) diseases that might cause distortion of the thoracic aortic morphology (pulmonary nodules with a diameter > 3 cm, mediastinal masses or lymph nodes with a diameter > 1 cm, pneumothorax, pulmonary bullae with a diameter > 3 cm, history of thoracic and mediastinal surgery, etc.); and (7) diseases that might cause distortion of the shape of the thoracic wall (scoliosis, barrel chest, pectus carinatum, history of spinal surgery, etc.) [21].

Imaging data were retrospectively retrieved from the continuous medical records of patients with healthy aortas who underwent chest CTA examination in four centers from April 2018 to December 2018 and included

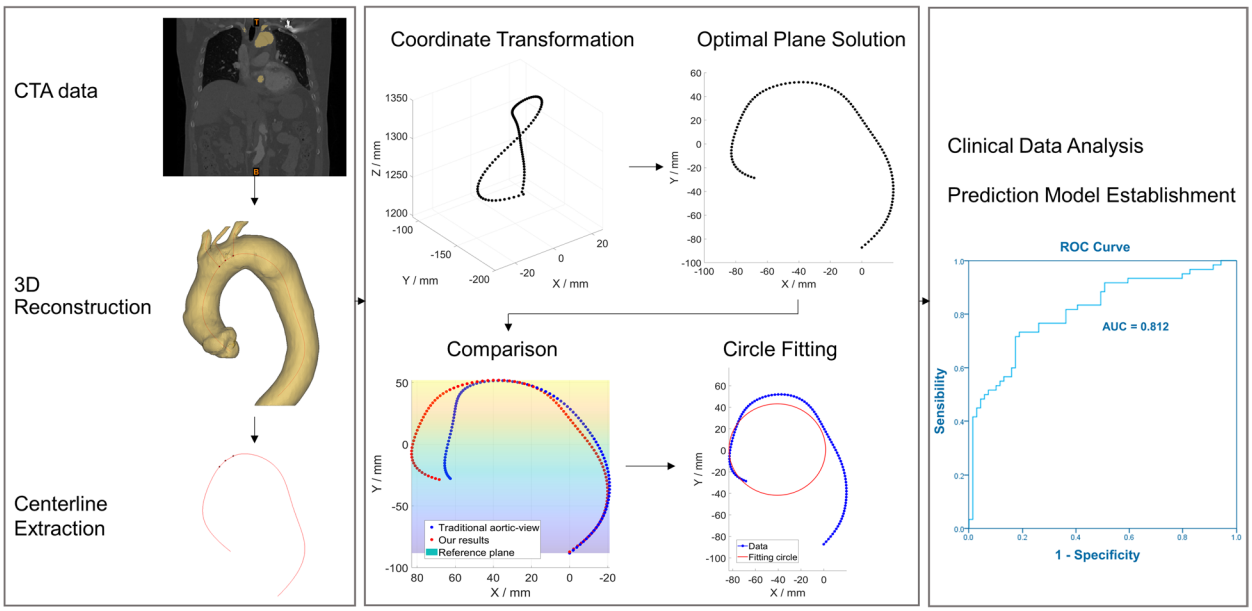



**Fig. 1** Flow chart of the study

in the healthy control group. The exclusion criteria for the healthy control group were as follows: (1) existing or previous aortic diseases (aortic dissection, aneurysms, coarctation of the aorta, etc.); (2) a previous cardiothoracic disease or cardiothoracic surgery; (3) diseases that might cause distortion of the thoracic aortic morphology (pulmonary nodules with a diameter > 3 cm, mediastinal masses or lymph nodes with a diameter > 1 cm, pneumothorax, pulmonary bullae with a diameter > 3 cm, history of thoracic and mediastinal surgery, etc.); and (4) diseases that might cause distortion of the shape of the thoracic wall (scoliosis, barrel chest, pectus carinatum, history of spinal surgery, etc.)

## Three-dimensional reconstruction of the aorta

### *Imaging*

A Toshiba 64-slice CT scanner (Toshiba Medical Systems (China), Beijing, China) was used with a scanning range from the entrance of the thorax to the lower boundary of the lung. Nonenhanced scanning was performed first, followed by contrast-enhanced scanning. Files were saved in DICOM format and anonymized. The raw DICOM format CTA data were imported into reconstruction software.

### *Three-dimensional reconstruction of aorta*

Two-dimensional cross-sectional images were adjusted to allow segmentation of the thoracic aorta in the segment module. The aorta was subjected to initial threshold segmentation according to dynamic area growth. Then, the calculate 3D function was used to reconstruct the processed mask in 3D. Afterward, the 3D model was smoothed to reduce spurious noise and maintain a biological shape. For the dissected aorta, dynamic area growth was used for the true and false lumen regions separately. After segmentation, the masks of the two parts were combined into one mask using the Boolean function under Boolean Operation. To facilitate the subsequent centerline extraction, the mask of the rupture site was repaired using Editing Masks and Multiple Slice to create a complete lumen.

## Aortic centerline extraction and centerline coordinate construction

The centerline was extracted semiautomatically according to the reconstructed 3D thoracic aorta model using Mimics software. The distance between the control points was 3 mm, and the coordinates of the thoracic aortic centerline were kept between 100 and 150. The entire thoracic aorta was divided into 6 segments according to Society for Vascular Surgery (SVS) segmentation standards (Zone 0: ascending aorta, including the innominate, Zone 1: from the distal edge of the innominate to the distal edge of the left common carotid, Zone 2: from the distal edge of the left common carotid to the distal edge of the left subclavian, Zone 3: first 2 cm distal to the left subclavian, Zone 4: from Zone 3 to the mid-descending thoracic aorta, Zone 5: mid-descending aorta to the proximal edge of the celiac artery) [22]. The coordinates from Zone 0 to Zone 4 were incorporated into the

following calculations. The coordinates of the dissected segments of the aorta were labeled 1, and the coordinates of the undissected segments were labeled 0.

### Determination of the optimal projection plane and circle fitting

As described in our previous study [3], the optimal projection plane can be determined according to the 3D coordinate transformation algorithm using MATLAB (2022, Mathworks, Inc.). The sum of absolute residuals (SAR) was used as the evaluation parameter, the XOY plane was used as the projection plane, and the two corresponding angles of rotation can be obtained. The best morphology of the corresponding projection plane can be obtained by rotating the original aortic centerline by the angle of rotation. The resulting 2D aortic morphology was segmented according to the six SVS classification criteria [22], and circle fitting was performed.

The improved algorithm of least-squares fitting using "area difference" was used to minimize the sum of the squares of errors and find the optimal function match. The coordinates of the fitted circle center are $(A, B)$, the radius is $R$, the sample size is $N$, the sample set is $(X_i, Y_i), i = 1, 2, 3, \ldots, N$, and the distance between the sample set and the center of the circle is $d_i$.

The equation of the fitted circle can be expressed as.

$$R^2 = (x-A)^2 + \left(y-B\right)^2 = x^2 - 2Ax + A^2 + y^2 - 2By + B^2. \tag{1}$$

Let $a = -2A, b = -2B, c = A^2 + B^2 - R^2$; then, the general equation of the circle is

$$x^2 + y^2 + ax + by + c = 0. \tag{2}$$

The center $(A, B)$ and radius $R$ can be obtained by reverse calculation $A = -\frac{1}{2}a, B = -\frac{1}{2}b, R = \frac{1}{2}\sqrt{a^2 + b^2 - 4c}$.

For the sample set $(X_i, Y_i)$, the squared distance from each point to the center of the circle is

$$d_i^2 = (X_i - A)^2 + (Y_i - B)^2. \tag{3}$$

The difference of squares $\delta_i$ between the distance from each point to the edge of the circle and the radius of the circle is

$$\begin{aligned}\delta_i &= d_i^2 - R^2 = (X_i - A)^2 + (Y_i - B)^2 - R^2 \\ &= X_i^2 + Y_i^2 + aX_i + bY_i + c.\end{aligned} \tag{4}$$

$Q(a, b, c)$ is the sum of the squares of $\delta_i$; then,

$$Q(a,b,c) = \sum \delta_i^2 = \sum \left(X_i^2 + Y_i^2 + aX_i + bY_i + c\right)^2. \tag{5}$$

When $Q(a, b, c)$ takes the minimum (min) value, it indicates that the current fitted circle is the closest to the sample distribution and thus the optimal fitted circle. Then, the partial derivatives of the parameters $a$, $b$, and $c$ for $Q(a, b, c)$ can be calculated, and the extreme points can be obtained by setting the partial derivative to 0. The minimum value can be obtained after comparing all of the extreme points.

The degree of agreement between the fitted circle and the sample data was analyzed. The sum of the squared error (SSE) was used to describe the degree of discreteness.

$$SSE = \sum (X_i - \overline{X})^2 \tag{6}$$

The length of the aorta is associated with the degree of discreteness but is also influenced by body size. Therefore, the radius of the fitting circle was proposed to eliminate the influence of body size on the degree of discreteness. The ratio of SSE to radius could be expressed as $\frac{1}{R}\sum (X_i - \overline{X})^2$, and the ratio of variance to the radius was calculated by $\frac{1}{NR}\sum (X_i - \overline{X})^2$.

### Clinical data analysis and correlation verification

Clinical data were processed with SPSS software (IBM SPSS 23.0, *SPSS* Inc.). All quantitative data are expressed as the mean ± standard deviation (SD), and the unpaired t test was used for comparisons between quantitative data. The correlation between the fitted circle and AD was tested using logistic regression models. The logistic regression model was adjusted by known risk factor of AD (age, sex, and hypertension) according to guideline and body size parameter (body surface area, BSA) which may affect aortic morphologic parameters [5]. BSA = 0.0061 × height (cm) + 0.0128 × weight (kg) − 0.1529. A receiver operative characteristic (ROC) curve was generated for the model. The predictive ability of the indicators was evaluated using the area under the curve (AUC), sensitivity, specificity, negative and positive predictive values. The cutoff value was calculated by ROC curve based on the best Youden's index. The baseline prevalence of AD was from previous reported rate of AD patients in patients presenting with symptoms concerning for AD in whom physicians ordered a CT specifically for the purpose of ruling in/out AD [23]. Statistical significance was considered at $P < 0.05$.

## Results

### Characteristics of involved population

CTA records of 98 AD patients were complete and available, among them 63 records were involved in the

analysis (22 samples with type A AD, and 41 samples with type B AD), and 71 samples from healthy people were involved. The average age of the AD group and control group was 56.90 ± 13.56 and 61.07 ± 17.16, respectively ($p = 0.095$). Between two groups, there were significant differences in the ratio of male (84.1% vs. 52.1%, $p < 0.001$), height (169.08 ± 8.07 vs. 163.29 ± 8.45, $p < 0.001$), weight (67.73 ± 13.18 vs. 61.40 ± 12.14, $p = 0.014$), BSA (1.75 ± 0.19 vs. 1.64 ± 0.20, $p = 0.0026$), and the ratio of hypertension patients (76.2% vs. 57.7%, $p = 0.029$) (Table 1). Considering that male sex and hypertension are risk factors for AD, this difference at baseline was not unexpected. These features may affect fitting-circle statistics and were supposed to be considered in our prediction model.

**Table 1** Characteristics of involved patients

| Characteristic | AD (63) | Healthy control (71) | *P* value |
|---|---|---|---|
| Male | 84.1% (53/63) | 52.1% (37/71) | < 0.001 |
| Age (year) | 56.90 ± 13.56 | 61.07 ± 17.16 | 0.095 |
| Height (cm) | 169.08 ± 8.07 | 163.29 ± 8.45 | < 0.001 |
| Weight (Kg) | 67.73 ± 13.18 | 61.40 ± 12.14 | 0.014 |
| Body surface area | 1.75 ± 0.19 | 1.64 ± 0.20 | 0.003 |
| Hypertension | 76.2% (48/63) | 57.7% (41/71) | 0.029 |
| Diabetes | 3.2% (2/63) | 7.0% (5/71) | 0.447 |
| Smoke | 9.5% (6/63) | 19.7% (14/71) | 0.144 |

Comparison of general characteristics of AD and control groups. *AD* aortic dissection. Body surface area = 0.0061 × height (cm) + 0.0128 × weight (Kg) − 0.1529

### The optimal plane projection solution

The spatial transformation process is shown in Fig. 2. Figure 2A shows the original 3D morphology of the aorta. The intermediate state shown in Fig. 2B can be obtained after matrix transformation using the first angle of rotation, and the optimal morphology Fig. 2C can be obtained through matrix transformation using the second angle of rotation. Figure 2D are the projections of the centerline onto the projection plane of XOY. After two transformations, the optimal aortic spatial morphology (i.e., the shape of a streamlined question mark), which minimizes the spatial entanglement of the aorta itself and yields the 2D morphology of the expanded aorta, can be obtained on the projection plane required for the aortic view.

### Aorta fitting result and circle-fitting distinctions of the thoracic aorta

The expanded aortic centerline of healthy aorta (Fig. 3A) and dissected aorta (Fig. 3B) was used to circle fitting. The coordinates of the center and the radius of the fitting

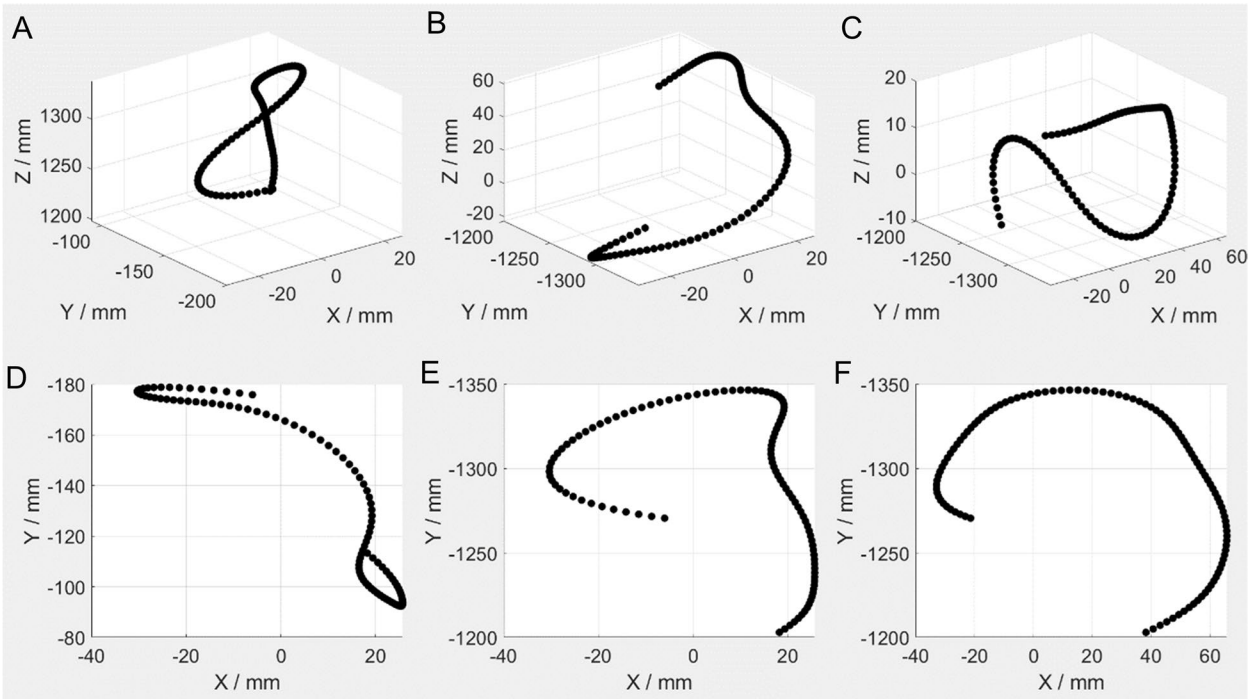



**Fig. 2** The process of the spatial transformation of the aortic centerline. **A** The original 3D morphology of the aorta. **B** The 3D morphology after the first rotation. **C** The optimal morphology after the second rotation. **D**-**F** are the projections of (a) onto the projection plane of XOY

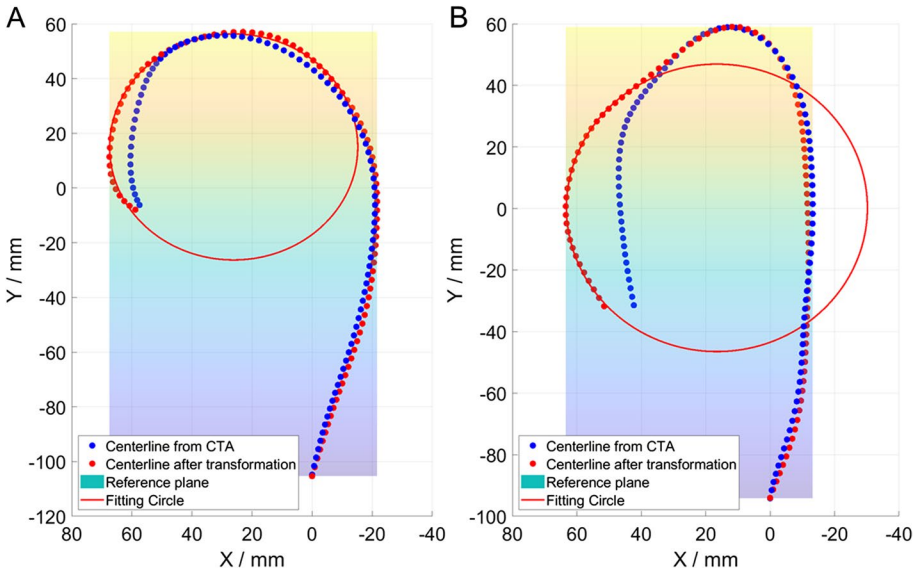



**Fig. 3** The representative diagram of the fitting circle of aorta. The aortic centerline of healthy aorta (**A**) and dissected aorta (**B**) in CTA (blue) and expanded aortic centerline after spatial transformation (red). The optimal aortic view was represented by the colored background

**Table 2** The fitting circle parameters

| Circle-fitting statistics | AD (63) | Healthy control (71) | *P* value |
|---|---|---|---|
| Sum of residuals | 5404.78 ± 3891.69 | 3502.45 ± 2566.71 | 0.001 |
| Variance | 129.90 ± 90.09 | 86.23 ± 56.60 | 0.001 |
| Radius of fitting circle | 45.63 ± 7.43 | 43.30 ± 6.78 | 0.061 |
| Variance/radius | 3.04 ± 2.65 | 2.04 ± 1.36 | 0.006 |

Distinctions of circle-fitting parameters in ascending aorta and aortic arch between dissection and healthy control groups

**Table 3** Results of logistic regression analysis

| Factors | OR (95% CI) | β value | *P* value |
|---|---|---|---|
| Variance/Radius (Fitting Circle) | 1.350 [1.023,1.782] | 0.300 | 0.034 |
| Age | 0.959 [0.932,0.987] | -0.042 | 0.005 |
| Sex | 3.842 [1.465,10.073] | 1.346 | 0.006 |
| Hypertension | 3.144 [1.265,7.810] | 1.145 | 0.014 |
| BSA | 7.670 [0.935,62.945] | 2.037 | 0.058 |
| Constant | 0.029 | -3.529 | 0.065 |

Multivariable logistic regression analysis of thoracic aorta fitting circle prediction model for aortic dissection. Regression model was adjusted for age, sex, hypertension and BSA. *CI* confidence interval, *OR* odds ratio, *BSA* body surface area

circle were obtained via solving the parameters a, b, and c of $Q(a, b, c)$. The representative diagram of the fitting circle of the healthy and dissected aorta was shown. The fitting circle parameters are listed in Table 2. The sum of residuals and variance was used to reflect the extent of similarity between the centerline of the thoracic aorta and the fitting circle. The sum of residuals was significantly higher in the AD group (5404.78 ± 3891.69 vs. 3502.45 ± 2566.71, $p = 0.001$). The variance of the fitting circle was also higher in the AD group (129.90 ± 90.09 vs. 86.23 ± 56.60, $p = 0.001$). Considering the non-negligible differences in sex and body size between the samples, the radius of the fitting circle was calculated (45.63 ± 7.43 vs. 43.30 ± 6.78, $p = 0.061$), and the variance divided by radius (3.04 ± 2.65 vs. 2.04 ± 1.36, $p = 0.006$) were used for AD prediction model.

### Fitting circle prediction model

According to the above comparisons of fitting circle statistics and sample baselines, variance/radius, age, sex, hypertension, and BSA are involved in logistic regression analysis (Table 3). The receiver operating characteristic (ROC) curve was used to assess the performance of this model. The area under the ROC curve (AUC) was 0.812 (Fig. 4). The optimum cutoff value was 0.545, and the sensitivity and specificity of the model derived from circle fitting were 73.3% and 81.2%, respectively. The negative predictive value of this model is 91.6% and the positive predictive value is 52.2%. The result of logistic regression analysis indicated that the variance/radius of the fitting circle was positively correlated with the probability of AD (OR = 1.350, β = 0.300, $p = 0.034$, the OR of variance/radius refers to the risk per 1-unit increase). The results matched the hypothesis: The shape of a healthy thoracic aorta could be reflected by a circle, while the shape of the aorta of AD patients did not fit the circle well.

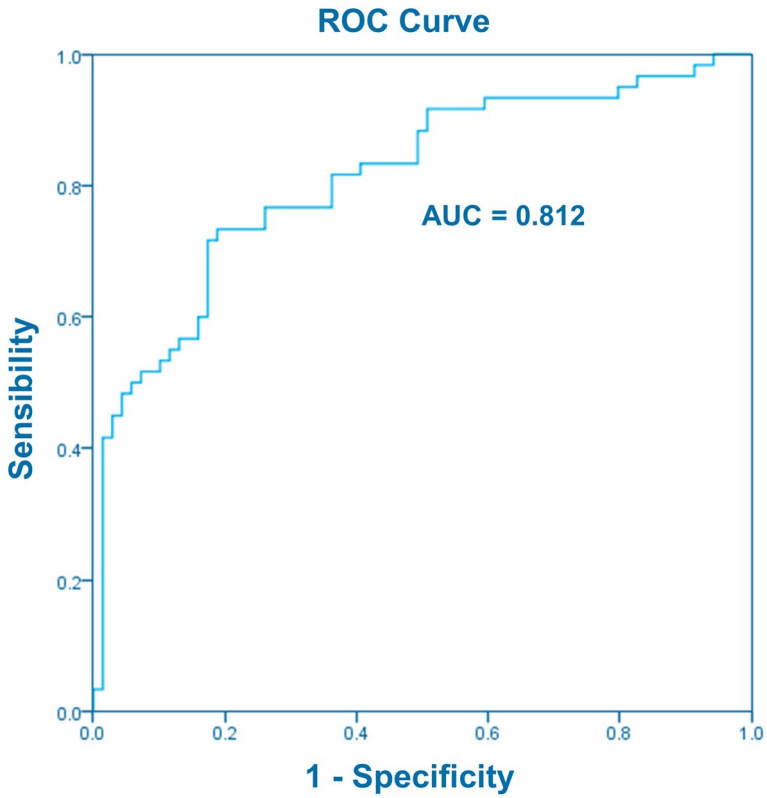



**Fig. 4** The ROC curve of the fitting circle prediction model. The AUC = 0.812. AUC: area under curve; ROC: receiver operating characteristic

## Discussion

This study demonstrated a significant difference between dissected and healthy aortas. As shown in Fig. 3, the shape of the healthy ascending aorta, aortic arch, and part of the descending aorta resembles a circle, while that of the dissected aorta differs from a circle. This degree of mismatch between the centerline and the fitted circle reflects the tortuosity and slumpedness of the aorta, which is consistent with observations in clinical practice. Considering the clinical needs, the baseline prevalence of AD in patients presenting with symptoms concerning for AD and received CT specifically for AD diagnose (21.9%) [23] was used to calculate predictive values. The negative predictive value (91.6%) is high, while due to reasons including low prevalence of AD, the positive predictive value (52.2%) is relatively low.

Based on this result, we proposed a new question: Can aortic dissection be identified high-dimensional morphological indicators describing the degree of local aortic deformation? By answering this question, patients with a high risk of dissection can potentially be identified. In this study, the optimal plane was confirmed mathematically; viewed from this optimal plane, the degree of mismatch between the centerline and the fitted circle was used to quantitatively describe the morphological characteristics of the aorta. The result suggested that this indicator achieved good performance in identifying AD.

According to previous studies, morphological risk factors for AD can be evaluated by the aortic centerline of AD patients. Rylski et al. compared the geometry features before and after aortic dissection onset. This study involved 63 non-Marfan patients with nonbicuspid aortic valves who had undergone computed tomography angiography < 2 years before and within 12 h after aortic dissection onset. The result indicated that while the largest increase in diameter and volume induced by the dissection were observed, the centerline length showed no significant difference before and after onset in ascending aorta (99.6 vs.105.0, $p = 0.090$), aortic arch (39.8 vs.41.0, $p = 0.677$) and proximal descending thoracic aorta (123.2 vs. 125.8, $p = 0.912$) [24]. Although the sample size of this study needs to be further expanded, it provides strong evidence for the consistency of the aortic centerline before and after onset. Similarly, Trimarchi et al., reported that the diameter of the aorta increases sharply after aortic dissection while the index extracted from the centerline is relatively stable to aortic dissection [14]. Based on this, multiple cross-sectional studies have used morphological features of the aortic centerline to identify the risk factors or predictors for aortic dissection. Using

the centerline method, Sun et al. reported that the incremental aortic arch angulation, the tortuosity, and the type III arch configuration are valuable geometric risk factors for type B dissection [25]. Corte et al. reported that along with aortic diameter and length, the asc-arch angle is a promising measurement to predict aortic dissection [20]. Another mainstream computer-aided diagnosis and treatment is achieved by segmenting the true and false lumen of aorta in AD patients, and there has been a wealth of positive results [25]. In 2006, Kovács et al. introduced model-based approaches to identify the true and false lumen of AD by the successive steps: segmentation of the aorta, detection of the intimal flap and identification of the two lumina [26]. Since each step is highly dependent on the preceding steps, the approach prone to failure on irregularly-shaped aortas. Besides, Lee et al. introduced an approach combines multi-scale wavelet analysis and generative-discriminative model matching to segment the lumens [27]. In recent years, deep learning has been an emerging approach to segment dissected aorta. Li et al. reported the first application of deep learning in AD, using two 2D cascaded convolutional networks to extract the contours of aorta and true lumen. Only the lumen contours are manually annotated with a fixed number of points [28]. Cao et al. designed a 3D U-Net that can segment true and false lumen simultaneously in a unified network, based on a large and manually annotated CTA datasets [29]. Based on previous studies, we presented the concept of the fitting circle using the centerline method. However, this evaluation of aortic geometry needs to be tested on a dataset that, for each subject, contains pre- and post-dissection imaging before any real predictive or risk-stratifying capability is claimed.

Furthermore, previous studies have indicated that the pathological changes in AD are not limited to the entry tear; rather, the whole aorta is affected and deformed [2, 21, 24]. These results raise new research questions for current aortic treatment: Does aortic stent implantation, which simply seals intimal tears, play the same role as "radical surgery" in aortic dissection? The onset of aortic dissection may be the result of pathological changes in the long section of the aorta. These pathological processes can lead to macroscopic deformation in properties such as the slumpedness, angulation, and stiffness of the aorta. In this case, we should pay attention to the general health of the aorta rather than only the intima tear.

Several limitations need to be acknowledged. The major shortcoming is that the sample size is relatively small. Larger sample size is required to draw more robust and accurate conclusions. Another shortcoming is that no external validation was performed. An independent cohort is needed to verify the conclusions. This series of studies is continuing, which may solve the above issues. Furthermore, we hope that this discrepancy will allow for rapid identification of thoracic AD at the onset, or even as a risk factor to predict AD before the onset. However, subgroup analyses based on interval from AD onset to CTA were not conducted. Therefore, although the parameter of fitted circle can describe the abnormalities associated with AD, it is unknown whether these parameters can identify early AD. Subgroup analysis is necessary after sample size increases. In addition, considering that the aim is to identify thoracic AD early, it would be more valuable if the control sample was people who had chest pain and in whom CTA was performed to rule out dissection, instead of healthy people. This could better reflect the situation in emergency and outpatient. Naturally, it is too early to consider such remote limitations in clinical practice based only on theoretical results. However, if new morphological indexes are proven to be superior to the current traditional diameter index in clinical practice, they may have the potential to form part of a new aortic dissection prevention and diagnose program.

We are committed to applying this work to the clinic. We established this reproducible approach by identifying SAR as the evaluation standard and obtaining the optimal 2D morphology with unified algorithms. Based on the current algorithm, we are developing software that can automatically calculate fitted circle parameters from CTA data. This tool would facilitate the expansion of sample size and the clinical application of the fitted circle model. In addition, other high-dimensional morphological indicators, such as collapse degree, are also considered in this tool.

## Conclusion

The morphological characteristics of the thoracic aorta can be described by a fitted circle, while that of the dissected aorta had poorer similarity to a circle. The fitting circle model is an effective indicator for dissected thoracic aortas.

### Abbreviations

| | |
|---|---|
| 2D | Two-dimensional |
| 3D | Three-dimensional |
| AD | Aortic dissection |
| AUC | Area under the curve |
| BSA | Body surface area |
| CT | Computed tomography |
| CTA | Computed tomography angiography |
| IRB | Institutional Review Board |
| ROC | Receiver operative characteristic |
| SAR | Sum of absolute value of residuals |
| SD | Standard deviation |
| SVS | Society for Vascular Surgery |

### Acknowledgements

None.

**Authors' contributions**
Hongji Pu: Investigation, Validation, Formal analysis, Resources, Writing - original draft. Tao Peng: Conceptualization, Methodology, Validation, Formal analysis, Writing - original draft. Zhijue Xu: Methodology, Validation, Writing - review& editing. Qi Sun: Methodology, Validation, Writing - review & editing. Zixin Wang: Methodology, Validation, Writing - review & editing. Hui Ma: Methodology, Validation, Writing - review & editing. Shu Fang: Methodology, Validation, Writing - review & editing. Yang Yang: Formal analysis, Writing - review & editing. Jie Wu: Methodology, Validation, Writing - review & editing. Ruihua Wang: Methodology, Supervision, Writing - review & editing. Peng Qiu: Conceptualization, Methodology, Validation, Formal analysis, Writing - original draft. Jinhua Zhou: Funding acquisition, Methodology, Supervision, Writing - review & editing. Xinwu Lu: Funding acquisition, Methodology, Supervision, Writing - review & editing.

**Funding**
This work was supported by Natural Science Foundation of China (82300540, 82170509, 82370494, 82170411) for data collection, data processing and software development, Natural Science Foundation of Anhui Provincial Education Department (KJ2021A0251) for data processing and data analysis, Clinical Research Program of 9th People's Hospital (JYLJ202010, JYLJ202204) for data collection and data processing, Shanghai Jiao Tong University School of Medicine Doctoral Innovation Fund (BXJ201935) for software development, Translational Medicine Science and Technology Infrastructure Opening Project (TMSK-2021-121) for software development, Shanghai Science and Technology Innovation Action Plan (20Y11909600, 21S31904300, 21Y11909500) for data analysis, Clinical Research Plan of SHDC (SHDC2020CR6016-003) for data processing, Shanghai Ninth People's Hospital Nursing Fund Project (JYHL2020MS01) for data analysis, Shanghai Municipal Health Bureau Project (202040434, 20224Y0170, 202240145) for data processing, Research Foundation of Anhui Medical University (2020xkj016) for data collection, and Research Fund of Anhui Institute of translational medicine (2021zhyx-B16, 2023zhyx-C53) for data processing.

**Availability of data and materials**
The datasets generated and/or analyzed during the current study are temporarily not publicly available due to the series of studies is ongoing. Data are now available from the corresponding author (Xinwu Lu) on reasonable request, and will also be publicly available after the series of studies are completed.

## Declarations

**Ethics approval and consent to participate**
The study protocols were approved by the Medical Ethics Committee of Shanghai Ninth People's Hospital Affiliated to Shanghai Jiao Tong University School of Medicine and Anhui Medical University, Institutional Review Board (IRB) approval number: SH9H-2019-T144-2. This study is registered in the Chinese Clinical Trial Registry (Registration Number: ChiCTR2000029219). Written informed consent was obtained from all participants. All methods were performed in accordance with STARD and Declaration of Helsinki.

**Consent for publication**
Not applicable.

**Competing interests**
The authors declare no competing interests.

Received: 21 March 2023 Accepted: 19 August 2024
Published online: 28 August 2024

**References**

1. Nienaber CA, Clough RE. Management of acute aortic dissection. Lancet. 2015;385(9970):800–11.
2. Evangelista A, Isselbacher EM, Bossone E, Gleason TG, Eusanio MD, Sechtem U, et al. Insights from the international registry of acute aortic dissection: a 20-year experience of collaborative clinical research. Circulation. 2018;137(17):1846–60.
3. Peng T, Pu H, Qiu P, Yang H, Ju Z, Ma H, et al. A stable and quantitative method for dimensionality reduction of aortic centerline. Front Cardiovasc Med. 2022;31(9):940711.
4. Hibino M, Otaki Y, Kobeissi E, Pan H, Hibino H, Taddese H, et al. Blood pressure, hypertension and the risk of aortic dissection incidence and mortality: results from the Japan-Specific Health checkups study, the UK biobank study and a meta-analysis of cohort studies. Circulation. 2022;145(9):633–44.
5. Isselbacher EM, Preventza O, Hamilton Black J 3rd, Augoustides JG, Beck AW, Bolen MA, et al. 2022 ACC/AHA guideline for the diagnosis and management of aortic disease: a report of the American Heart Association/American College of Cardiology Joint Committee on Clinical Practice guidelines. Circulation. 2022;146(24):e334-482.
6. Dasi LP, Pekkan K, de Zelicourt D, Sundareswaran KS, Krishnankutty R, Delnido PJ, et al. Hemodynamic energy dissipation in the cardiovascular system: generalized theoretical analysis on disease states. Ann Biomed Eng. 2009;37(4):661–73.
7. Fukuta H, Little WC. The cardiac cycle and the physiologic basis of left ventricular contraction, ejection, relaxation, and filling. Heart Fail Clin. 2008;4(1):1–11.
8. Sommer G, Gasser TC, Regitnig P, Auer M, Holzapfel GA. Dissection properties of the human aortic media: an experimental study. J Biomech Eng. 2008;130(2):021007.
9. Yu X, Suki B, Zhang Y. Avalanches and power law behavior in aortic dissection propagation. Sci Adv. 2020;6(21):eaaz1173.
10. Nienaber CA, Eagle KA. Aortic dissection: new frontiers in diagnosis and management: part I: from etiology to diagnostic strategies. Circulation. 2003;108(5):628–35.
11. Lee JH, Kim J, Lee SJ, Kim YA, Maeng YI, Park KK. Apoptosis and fibrosis of vascular smooth muscle cells in aortic dissection: an immunohistochemical study. Int J Clin Exp Pathol. 2020;13(8):1962–9.
12. Haslach HW Jr, Siddiqui A, Weerasooriya A, Nguyen R, Roshgadol J, Monforte N, et al. Fracture mechanics of shear crack propagation and dissection in the healthy bovine descending aortic media. Acta Biomater. 2018;68:53–66.
13. Pape LA, Tsai TT, Isselbacher EM, Oh JK, O'gara PT, Evangelista A, et al. Aortic diameter > or = 5.5 cm is not a good predictor of type A aortic dissection: observations from the International Registry of Acute Aortic dissection (IRAD). Circulation. 2007;116(10):1120–7.
14. Trimarchi S, Jonker FH, Hutchison S, Isselbacher EM, Pape LA, Patel HJ, et al. Descending aortic diameter of 5.5 cm or greater is not an accurate predictor of acute type B aortic dissection. J Thorac Cardiovasc Surg. 2011;142(3):e101-10715.
15. Heuts S, Adriaans BP, Gerretsen S, Natour E, Vos R, Cheriex EC, et al. Aortic elongation part II: the risk of acute type a aortic dissection. Heart. 2018;104(21):1778–82.
16. Adriaans BP, Heuts S, Gerretsen S, Cheriex EC, Vos R, Natour E, Maessen JG, et al. Aortic elongation part I: the normal aortic ageing process. Heart. 2018;104(21):1772–7.
17. Heuts S, Adriaans BP, Rylski B, Mihl C, Bekkers S, Olsthoorn JR, et al. Evaluating the diagnostic accuracy of maximal aortic diameter, length and volume for prediction of aortic dissection. Heart. 2020;106(12):892–7.
18. Shirali AS, Bischoff MS, Lin HM, Oyfe I, Lookstein R, Griepp RB, et al. Predicting the risk for acute type B aortic dissection in hypertensive patients using anatomic variables. JACC Cardiovasc Imaging. 2013;6(3):349–57.
19. Sun L, Li J, Wang L, Li Q, He H, Li X, et al. Aortic geometric alteration associated with acute type B aortic dissection: angulation, tortuosity, and arch type. Front Physiol. 2021;12:708651.
20. Della Corte A, Rubino AS, Montella AP, Bancone C, Lo Presti F, Galbiati D, et al. Implications of abnormal ascending aorta geometry for risk prediction of acute type a aortic dissection. Eur J Cardiothorac Surg. 2021;60(4):978–86.
21. Qiu P, Liu J, Chen Y, Zha B, Ye K, Qin J, et al. Changes in aortic arch geometry and the risk for Stanford B dissection. J Thorac Dis. 2020;12(12):7193–201.
22. Lombardi JV, Hughes GC, Appoo JJ, Bavaria JE, Beck AW, Cambria RP, et al. Society for vascular surgery (SVS) and society of thoracic surgeons (STS) reporting standards for type B aortic dissections. J Vasc Surg. 2020;71(3):723–47.

23. Nazerian P, Giachino F, Vanni S, Veglio MG, Castelli M, Lison D, et al. Diagnostic performance of the aortic dissection detection risk score in patients with suspected acute aortic dissection. Eur Heart J Acute Cardiovasc Care. 2014;3(4):373–81.
24. Rylski B, Munoz C, Beyersdorf F, Siepe M, Reser D, Carrel T, et al. How does descending aorta geometry change when it dissects? Eur J Cardiothorac Surg. 2018;53(4):815–21. Sun L, Li X, Li Q, Li M, He H,Wang T, et.al. Morphological Features of Aortic Arch Predicting the Risk forAcute Type B Aortic Dissection. World J Surg 2021; 45(11):3458–66.
25. Pepe A, Li J, Rolf-Pissarczyk M, Gsaxner C, Chen X, Holzapfel GA, et al. Detection, segmentation, simulation and visualization of aortic dissections: a review. Med Image Anal. 2020;65:101773.
26. Kovács T, Cattin P, Alkadhi H, Wildermuth S, Székely G. Automatic segmentation of the vessel lumen from 3D CTA images of aortic dissection. In: Bildverarbeitung für die Medizin. Berlin, Heidelberg: Springer; 2006. p. 161–5.
27. Lee N, Tek H, Laine AF. True-false lumen segmentation of aortic dissection using multi-scale wavelet analysis and generative-discriminative model matching. SPIE Med Imaging. 2008;6915:878.
28. Li Z, Feng J, Feng Z, An Y, Gao Y, Lu B, et al. Lumen segmentation of aortic dissection with cascaded convolutional network. In: In: International workshop on statistical atlases and computational models of the heart. 2019. p. 122–30.
29. Cao L, Shi R, Ge Y, Xing L, Zuo P, Jia Y. Fully automatic segmentation of type B aortic dissection from CTA images enabled by deep learning. Eur J Radiol. 2019;121:108713.

## Publisher's note

Springer Nature remains neutral with regard to jurisdictional claims in published maps and institutional affiliations.